Selective Ion Acceleration by Intense Radiation Pressure

Contact: a.mcilvenny@qub.ac.uk

A. McIlvenny, H. Ahmed, P. Martin, S. Kar and M. Borghesi
Centre for Plasma Physics, Queen's University Belfast, Belfast BT7 1NN, United Kingdom

E. J. Ditter, O. C. Ettlinger, G. S. Hicks and Z. Najmudin
The John Adams Institute for Accelerator Science Imperial College London London SW7 2BZ, United Kingdom

A. Macchi
Dipartimento di Fisica Enrico Fermi, Università di Pisa, Pisa, Italy

D. Doria
Extreme Light Infrastructure (ELI-NP) and Horia Hulubei National Institute for R & D in Physics and Nuclear Engineering (IFIN-HH), Str. Reactorului No. 30, 077125 Bucharest–Măgurele, Romania

N. Booth, G. G. Scott, P. P. Rajeev and D. Neely
Central Laser Facility, Rutherford Appleton Laboratory, OX11 0QX, United Kingdom

S. D. R. Williamson and P. McKenna
SUPA, Department of Physics University of Strathclyde Glasgow G4 0NG, United Kingdom

L. Romagnani
LULI, École Polytechnique, CNRS, Route de Saclay, 91128 Palaiseau Cedex, France

Abstract

We report on preferential acceleration of heavy ions in an inherently multi-species target by the intense radiation pressure of the GEMINI laser incident on ultra-thin foils with circular polarization. At the optimum thickness of 15 nm, heavy ion (C^{6+}) energies were detected up to 33 MeV/nucleon and protons with a maximum energy cut off of 18 MeV. This difference, typically the opposite to what is observed with laser-foil interactions, is attributed (via multi-dimensional Particle in Cell simulations) to the removal of contaminant protons (and their subsequent thermal acceleration) by the laser's coherent contrast with the carbon ions being accelerated via Radiation Pressure Acceleration in the Light Sail regime. This is supported by the experimental measurement of different scaling of the maximum ion energy with laser intensity for the two species.

1 Introduction

Exploring novel laser-driven ion acceleration mechanisms is a key requirement for generation of ion beams of sufficient energy and quality for applications [1]. In particular, Radiation Pressure Acceleration (RPA) acting in the Light Sail (LS) regime is predicted to generate an inherently mono-energetic beams of bulk ions with high conversion efficiency and fast scaling with laser fluence [2, 3]. In typical laser-foil interactions this regime is inhibited due to excessive target heating and the dominance of other mechanisms such as Target Normal Sheath Acceleration (TNSA) and Relativistically Induced Transparency (RIT). However, this regime can be accessed by enhancing the laser contrast, using circular polarization (CP) at normal incidence and using ultra-thin foils (∼10 nm) [4–6].

Protons, with their higher Z/A ratio, are typically accelerated more efficiently than heavier ions in the electric fields generated in laser-solid interactions. However, the results presented here show that, under favourable conditions, it is possible to obtain the opposite results of a more efficient acceleration of preferentially accelerate the heavy bulk species by RPA-LS.

2 Experimental Set-Up and Results

The experiment was carried out with the north beam from GEMINI, temporally cleaned with a double plasma mirror arrangement producing a contrast of 10^{-14} on the 100's ps timescale and 10^{-6} at 1 ps. The wavefront was measured and improved with adaptive optics, to maximise the energy inside the 3 μm FWHM focal spot which was obtained with an $f/2$ off-axis parabola reaching a peak intensity of 5.5×10^{20} W/cm^2. The polarization was altered using a zero-order $\lambda/4$ waveplate placed in the re-collimated beam, after the plasma mirrors.

The primary ion diagnostics consisted of 3 Thomson Parabola Spectrometers (TPS) placed at -4°, 0° and 9°

with respect to the target normal (laser axis). These were coupled with Microchannel Plate detectors, to allow for remote and online data acquisition. Stacks of radiochromic film (RCF) were also used on dedicated shots to monitor the ion beam profile [7].

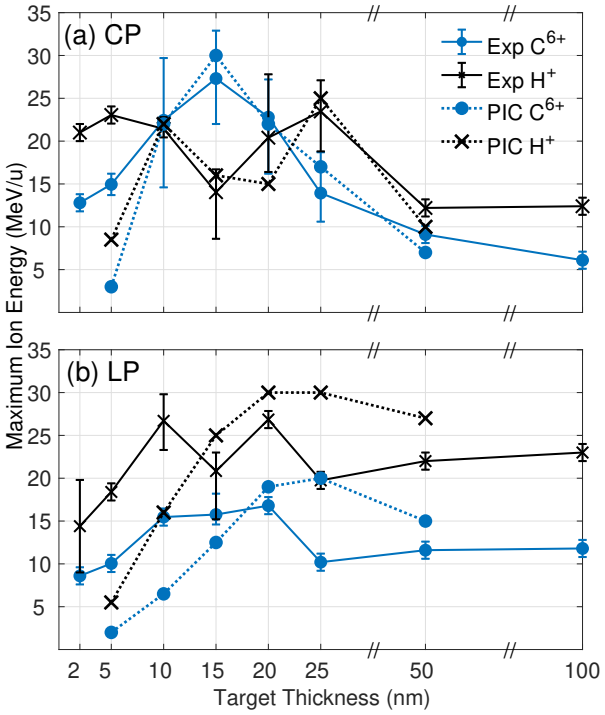

Figure 1: Maximum ion energy for the 0° TPS for C^{6+} (blue) and protons (black). The data is shown for (a) CP and (b) LP. The experimental data is shown with solid lines (and solid markers) and simulations with dotted lines (and empty markers) The errorbars represent the shot-to-shot variation in the measurement for shots $> 4 \times 10^{20}$ W/cm^2 due to laser energy fluctuations.

The results of the maximum ion energy observed for each species and laser polarization are shown in figure 1. Figure 1(a) highlights the presence of an optimal thickness at 15nm, where the C^{6+} energies are up to 33 MeV/nucleon (~400 MeV). Interestingly, under the conditions where the maximum carbon energies are obtained (15 nm and circular polarization), a local minimum is observed for the proton energies (18 MeV versus the 33 MeV/nucleon of C^{6+}). The intensity dependence of the maximum energy for the two ion species at the optimum thickness of 15 nm is shown in figure 2(a). While C^{6+} scales favourably with intensity ($E_{C^{6+}} \propto I^{1.2}$), H^+ follows a much slower trend. This behaviour is not observed for linear polarization (LP), shown in figure 2(b), where there is no clear peak in carbon energies and consistently higher proton energies for the same target thicknesses.

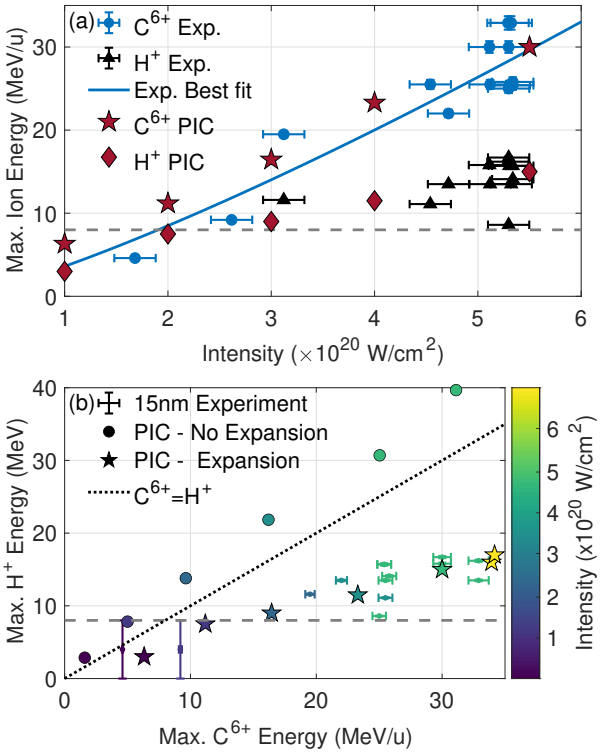

Figure 2: (a) Maximum ion energy as a function of laser intensity for experimental measurements of C^{6+} (blue circles) and H^+ (black triangles). Maximum energy from 2D PIC with expansion included are also shown for C^{6+} and H^+ with red stars and diamonds respectively. The solid line represents the best fit line to the C^{6+} experimental data, $\propto I^{1.2}$ (b) Correlation between C^{6+} and H^+ maximum energies for experimental and simulation data (marker colors indicate the laser intensity). Dotted line of $y = x$ (C^{6+}=H^+) acts as a guide showing that to the left, protons are preferentially accelerated, with carbon to the right. PIC simulations show that without expansion, H^+ energies are higher in this regime contrary to experimental data. With expansion included, the experimental trend is reproduced. The dashed line at y=8 MeV in (a) and (b) represents the detection threshold for protons only.

3 Simulations and Discussion

To understand this somewhat counter-intuitive behaviour, 2D Particle in Cell (PIC) simulations were performed using the EPOCH code [8]. The first case considered was that of a flat foil irradiated at normal incidence by a pulse with length 40 fs FWHM and transverse spatial profile of 3 μm FWHM. These simulations begin at time t=-100fs (where 0 fs is set by the peak of the pulse arriving at the target), and do not consider any of the coherent contrast and therefore represent an idealised scenario. The target was composed of C^{6+} neutralized with electrons at a density of 350n$_c$ (where n$_c$ is the critical density of ~1.75×10^{21}cm^{-3}) with front and rear surface,

5nm-thick 10n_c H^+ layers to simulate contaminant layers (where the H^+ from targets usually originate). The simulations were performed on a grid with resolution Δx = 5 nm, $\Delta y = 4\Delta x$, x-range [-10 μm, 30 μm]. The target was initially located at x=0, with y-range [-5 μm, 5 μm] and was initialized with 200 particles per cell per species with a temperature of 10 keV. Collisions are not calculated in this case as justified by their negligible influence at the temperature generated at this intensity. In these PIC simulations with an idealized pulse profile, the H^+ energies scale similarly to carbon albeit they are ∼30% higher (circles in figure 2(b)). These 2D simulations reproduce the I^2 scaling associated with LS-RPA since an idealized target at this thickness (without considering any significant pre-expansion) can enter the LS stage almost instantaneously and remain opaque for the majority of the pulse duration.

The observed deviation of each species' energy scaling with intensity between the experiment and idealized simulations, shown in figure 2(b), can be attributed to the target expansion before the main pulse arrives. In this experiment, a double plasma mirror arrangement was used for contrast enhancement as this significantly reduces target heating and expansion. The plasma mirrors are typically activated a few ps before the main pulse as the inherent contrast level decreases, meaning that the pulse is still preceded by a few ps of the coherent contrast. Considering this, a second series of simulations were performed including this preceding intensity. The same grid is initialized in these simulations except now with ionization and collisions calculated and the target set as unionized and cold.

At the optimum thickness, the interaction can be thought of as consisting of 3 stages: i) expansion ii) re-compression and iii) acceleration. The low intensity pedestal ionizes and heats the target that then expands (top image in figure 3). At this stage protons, with their lighter mass expand faster than the carbon ions and are mainly located in the front and rear underdense plasma. The target bulk has also expanded but it remains overdense.

In the final picosecond before the main pulse arrives, the radiation pressure begins to overcome the plasma's thermal pressure. The front surface is compressed and steepens the front density gradient, reversing some of the density decrease caused by the earlier expansion shown in the bottom image of figure 3; this affects only the overdense carbon plasma, as the protons are not present in significant number in this central region. Hot electrons, produced by the pulse's rising edge, begin to accelerate protons from the target rear and away from the compressed plasma region. When the pulse peak arrives, it interacts with a re-compressed (but reduced density) plasma which is close to the optimal areal density for the incident intensity. Here the laser accelerates the carbon bulk by RPA-LS whereas proton energies will be determined by the initial pre-expansion followed by sheath

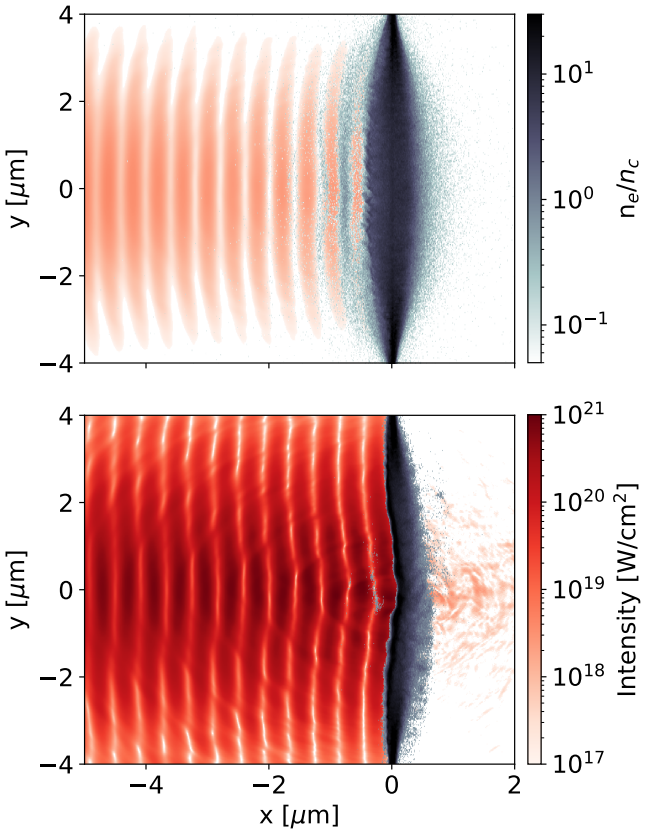

Figure 3: 2D PIC maps of electron density (grey scale) and laser intensity (red scale) at -83 fs (top) and -23 fs (bottom) with respect to the peak of the pulse hitting the target at 0 fs (each colourbar refers to both images). The laser enters from the left and is centred at y = 0 μm.

acceleration. As a result of these dynamics, the high energy carbon ions from the target bulk are accelerated much more efficiently than H^+.

The RPA-LS phase is followed by an RIT phase. Close to the peak of the pulse, the plasma becomes relativistically transparent (at time t_{RIT}=-3±3 fs). The interaction in the RIT regime also has a role in accelerating ions, and its importance can be estimated by a comparison with a simulation in which the pulse is cut just after the peak, at the end of the RPA stage. This comparison shows that the RIT regime accounts for ∼37% of the final C^{6+} energy and ∼63% of the final proton energy.

For LP, the resemblance between experimental and simulation data is less strong; this is likely to be due to the dimension dependence of the acceleration mechanisms in the expanded target; in 3D, one would expect the transition to transparency to occur earlier than in 2D thus favouring thinner targets and shifting the peak in the simulation trend closer to the experimental ob-

servation. For LP, where the transition to transparency occurs earlier ($t_{RIT} = -18 \pm 3$ fs) relative to CP, the effect of transparency enhanced acceleration is much more significant accounting for ∼76% of the final C^{6+} energies and ∼68% for protons.

The peak intensity was varied in the simulations to test the ion energy scaling as was done in the experiment. The scaling for both species obtained under these conditions matches the experiment more closely (compared to the idealized simulations), reproducing the observed species dependence. The simulations show that a reduced intensity scaling for carbon compared to the ideal I^2 dependence arises from the combination of two effects: 1) a delayed transition to LS since the initial hole boring phase must penetrate through the now expanded target; 2) an earlier transition to transparency for more intense pulses.

4 Conclusion

The data presented here confirms that the LS acceleration dynamics in ultrathin foils are highly sensitive to contrast levels on ps timescale. However, the data also indicates that it is possible to exploit the unavoidable coherent contrast in the laser system for moderate target expansion and acceleration of bulk ions. This regime demonstrates the potential of preferentially accelerating species other than protons extending the capabilities of dedicated systems for applications (e.g. radiobiology) such as the upcoming EPAC facility.

References

[1] A. Macchi *et al.* Ion acceleration by superintense laser-plasma interaction. *Reviews of Modern Physics*, 85(2):751–793, 2013.

[2] A. Macchi *et al.* "light sail" acceleration reexamined. *Physical Review Letters*, (8):1–4.

[3] S. Kar *et al.* Ion acceleration in multispecies targets driven by intense laser radiation pressure. *Physical Review Letters*, 109(18):1–5, 2012.

[4] C. Scullion *et al.* Polarization Dependence of Bulk Ion Acceleration from Ultrathin Foils Irradiated by High-Intensity Ultrashort Laser Pulses. *Physical Review Letters*, 119(5):1–6, 2017.

[5] A. Henig *et al.* Radiation-pressure acceleration of ion beams driven by circularly polarized laser pulses. *Physical Review Letters*, 103(24):3–6, 2009.

[6] A P L Robinson *et al.* Radiation pressure acceleration of thin foils with circularly polarized laser pulses. *New Journal of Physics*, 10(1):013021, 2008.

[7] C. Scullion *et al.* Angularly resolved characterization of ion beams from laser-ultrathin foil interactions. *Journal of Instrumentation*, 11(09):C09020–C09020, 2016.

[8] T. D. Arber *et al.* Contemporary particle-in-cell approach to laser-plasma modelling. *Plasma Physics and Controlled Fusion*, 57(11):113001, 2015.